View metadata, citation and similar papers at core.ac.uk
brought to you by CORE
provided by Repository@Nottingham

Installed Antenna Performance in Airborne Radomes of Different Profiles

Ana Vukovic, Phillip Sewell, Xuesong Meng, and Trevor M. Benson

George Green Institute for Electromagnetics Research, Department of Electrical and Electronic Engineering
University of Nottingham, Nottingham, NG7 2RD, UK
ana.vukovic@nottingham.ac.uk, xuesong.meng@nottingham.ac.uk, trevor.benson@nottingham.ac.uk,
phillip.sewell@nottingham.ac.uk

Abstract — In this paper, broadband interactions between an antenna and a radome are modelled using a full wave numerical solver. By accurately describing both the antenna and the radome geometry with a single numerical method, a comprehensive prediction of the performance of the coupled antenna and radome installation is provided. The paper compares how different airborne dielectric radome profiles affect the antenna performance, predicting effects not seen in uncoupled simulations.

Index Terms — Airborne radome, installed antenna, unstructured transmission line modelling method.

I. INTRODUCTION

Airborne radomes are weatherproof enclosures that protect antennas from the physical environment but are intended to have minimal impact on antenna performance. In practice, the aerodynamic requirements on a radome's profile compromises their benign nature for installed antenna performance; this typically manifests itself as an increase in the sidelobe level of the antenna radiation pattern and as a boresight error [1]. This is particularly true in cases where the antenna is installed close to the radome surface. In such scenarios, a better understanding of antenna-radome interactions is necessary for accurate predictions of deployed antenna performance.

Over the last decade, rapid progress in computational power and advances in distributed processing, mean that a number of numerical techniques are ever more capable of tackling larger and complex problems. Notwithstanding the advances in modelling capability, it is notable that the analysis of the electromagnetic interactions between antennas and radomes is still performed in a "decoupled" fashion, even for moderately sized problems, due to the multiscale nature of the antenna and the radome geometry [1, 2]. One common approach is to replace the intricate detail of the antenna geometry by a 3D surface of equivalent electric and magnetic currents [1]. Alternatively, the radiating fields from the antenna are computed without the radome and subsequent evaluation of the effect of the radome on the radiation pattern is performed using these fields as an excitation [1, 2]. In both approaches, decoupling the antenna from the radome means that their mutual interactions are not fully taken into account in the design and simulation cycle. It is immediately obvious that, in order to take full account of these interactions, a flexible, accurate and efficient broadband solver that can efficiently deal with the multiscale features and complex geometries of the problem is required.

In this paper we report on the application of the numerical time-domain Transmission Line Modelling (TLM) method to the fully-coupled modelling of the moderate size problem posed by radome-antenna interactions. Both the antenna and the radome are discretized within a single numerical method based upon an unstructured tetrahedral mesh, referred to as the Unstructured TLM (UTLM) method. The TLM method exploits the analogy between solutions of the 3D Maxwell's equations for electromagnetic fields and voltages and currents on an interconnected network of transmission lines to identify an explicit time stepping algorithm for the electromagnetic fields. Development of the TLM method for use with unstructured tetrahedral meshes was first reported in [3, 4] and has since been fully characterized. Unlike the finite difference and finite element time domain (FDTD, FETD) methods, the UTLM method is unconditionally stable, with stability strictly provable a priori on cell by cell basis. Late time instability is never observed and the explicit nature of the algorithm is highly efficient, without for example, introducing approaches such as mass lumping. TLM time stepping algorithms exhibit a high degree of concurrency, and hence, parallelize well on many-core processors systems. Use of tetrahedral meshes eliminates the numerical noise due to the staircase approximations to geometry typically found in the simplistic Cartesian TLM and FDTD methods. Moreover, smoother representations of curved geometrical boundaries and the inherent availability of graded meshes that permit efficient discretization of subwavelength features in large computational domains are also advantageous. The latter can be facilitated by either using a purely tetrahedral mesh, or more practically, by hybridizing

Submitted On: August 18, 2016
Accepted On: September 27, 2016

1054-4887 © 2016 ACES

computationally efficient cubic grids and tetrahedral meshes, e.g., [5].

In this paper, antenna-radome interactions are modelled in a fully coupled manner using the UTLM method. A single broadband Vivaldi antenna enclosed in a monolithic dielectric radome of moderate size is selected as the test case. Besides the discretization, the UTLM method makes no other approximation and as long as a sufficiently fine mesh is used to discretize the whole problem, we can be assured that all physical interactions are accounted for. The open end of the dielectric radome is mounted on a perfectly conducting surface consistent with practical airborne installations. In order to separate the effect of this mounting plate and the radome's profile, the effect of the presence of just this mounting plate on the antenna's performance is investigated before the radome itself is added to the model. Spherical, spherically blunted cone and two types of superspheroidal radomes are considered, and antenna-radome interactions are assessed in terms of the return loss, S_{11}, and the radiation patterns of the installed antenna. The paper is structured as follows. In the next section the antenna geometry mounted on just the conducting plate is described and modelled. Section III then assesses how different radome profiles affect the antenna's performance, and Section IV summarizes the main conclusions of the paper.

II. ANTENNA ON THE RADOME MOUNTING PLATE

In this section, the performance of the Vivaldi antenna described in [6] mounted on a moderate size conducting plate is described. The slot line is printed on a substrate of dielectric constant ε_{rs}=3 and is flared to provide a smooth impedance transition between the coaxial feed and free space. The half width of the slot line varies with distance as $w(z) = 0.25e^{0.0797z}$ reaching 20 mm at the wider end. A balun is realized as a void in the flared metallic region of radius 2.5 mm. The height, width and thickness of the dielectric substrate are 55 mm, 40 mm and 1.5 mm respectively. The perfectly conducting plate is cylindrical with radius 2 m and thickness 7 mm. The coaxial feed, designed to have a characteristic impedance of 50 Ω, has inner and outer radius of 1 mm and 3.495 mm, and dielectric constant of ε_{rc} =2.25. The problem space is surrounded by a fictitious surface of dimensions 4.8 m x 4.6 m x 6.2 m to both terminate the space with a free space radiation boundary condition and on which to capture the radiation fields. The antenna is excited with the TEM mode of the coaxial feed modulated by a time envelope to provide a center frequency of 3.2 GHz [6] and a bandwidth spanning 1.5 to 4.5 GHz.

An example of the antenna and radome mounting plate geometry is shown in Fig. 1 and the complete geometry with a radome is shown in the inset of the Fig. 1. The whole problem is meshed with a 5 mm cubic mesh to sample the free space region [6] in conjunction with a high quality tetrahedral mesh to capture the detailed geometry. Specifically, the surfaces of, and the space around, the antenna and feed cable shown in Fig. 1, are sampled by triangular and tetrahedral cells characterized by the figure of merit Q=2. (Cell Q is defined as the ratio between the circumradius to the minimum edge length of the cell and generally values less than 5 correspond to nicely shaped cells yielding good spatial sampling [7]).

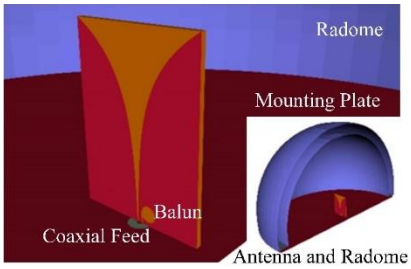

Fig. 1. Antenna on the radome mounting plate and antenna inside a radome in the inset of the figure.

Figure 2 presents S_{11} parameter for the antenna mounted on just the perfectly conducting plate. To assess the impact of mesh dispersion errors and sensitivity to the meshing in general, the simulation was also repeated using the mesh obtained when a *ghost* spherical half-wave dielectric radome of thickness of 24.2 mm, but of relative permittivity set to ε_r=1, is present. Physically, the radome is not electromagnetically present, but its geometry is still imprinted on the mesh. Finally, a spherical half-wave dielectric radome of permittivity ε_r=4.2 and wall thickness of 24.4 mm, designed to operate at 3 GHz was introduced. Figure 2 shows that there is no difference between the performance of the antenna on the just mounting plate, and with the *ghost* radome in place over the operating range, indicating no discernable sensitivity to the meshing. Moreover, this result agrees very well with that already reported in [6]. However, when for the first time, a fully coupled simulation is performed in the presence of the dielectric radome, it can be seen that S_{11} deteriorates over the operating range due to reflections form the radome. For reference, the computations simulated a total of 0.02 μs using a time step of Δt=0.01ps on 25 processor cores of a commodity cluster and required ~5.5 h to complete.

Figures 3 (a, b) compares the radiation patterns in the H- and E-plane for all three cases. Figure 3 (a) also shows the coordinate planes and the azimuthal H-plane denoted by angle ϕ and the elevation E-plane denoted by angle θ. Figure 3 shows that the radiation patterns for the antenna just on the mounting plate and with the *ghost* radome are identical, whereas the presence of the dielectric spherical radome causes stronger rippling in

the main beam of the H-plane pattern (ϕ=270 deg) and increased radiation in the sidelobe (θ=90 deg), as shown in Fig. 3 (a). The E-plane radiation pattern of the dielectric spherical radome shows slightly lower directivity compared to the antenna just on the mounting plate.

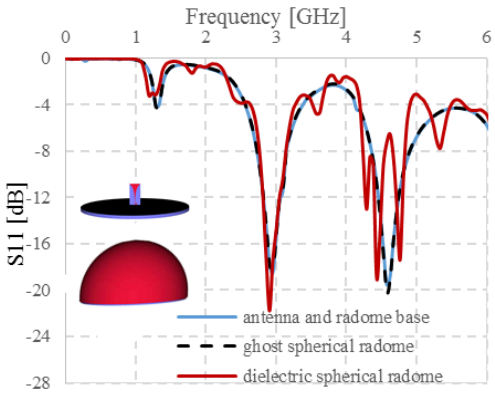

Fig. 2. S_{11} for the antenna on the mounting plate, with the *ghost* spherical radome and the dielectric spherical radome with ε_r=4.2.

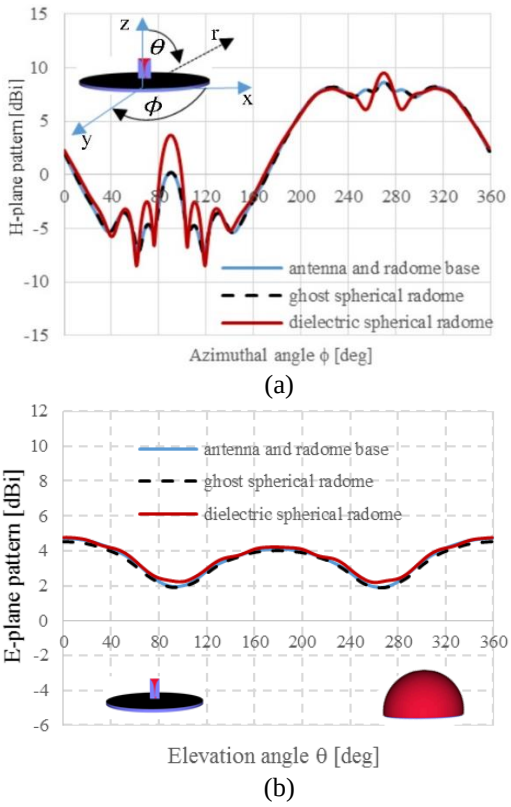

Fig. 3. (a) H-plane pattern and (b) E-plane radiation pattern for antenna on the radome base, with *ghost* spherical radome and the dielectric spherical radome.

III. IMPACT OF DIFFERENT RADOME PROFILES ON ANTENNA PERFORMANCE

In this section, the performance of the Vivaldi antenna installed in several different radomes is analyzed and compared with the case of antenna mounted on the radome base, i.e., without a radome. Illustrative aerodynamic radome profiles are chosen, namely, a spherically blunted cone and two superspheroidal profiles. In all cases, the radome's base radius and length are fixed to be R=2 m and L=2.2 m respectively. In all cases, the half-wave monolithic radome is made of a glass composite of thickness 24.4 mm and dielectric constant ε_r=4.2, which is designed to operate at 3 GHz. Radome losses are neglected. The cone profile radome is blunted by a sphere of radius 0.1 m. The superspheroidal radomes are described by the equation $x^2 + y^2 = \left(\frac{2R}{L}\right)^2 (L^p - z^p)^{2/p}$, where the coordinate z is defined along the axis of the radome, and parameter p defines the particular profile; p=1.449 and p=1.161 give the ogive and superspheroidal profiles of [2] respectively. All simulations were performed with the same meshing and run time parameters given in Section II.

Figure 4 assesses S_{11} in the operating range for the antenna installed in three different airborne radomes. The radome profiles are also given in Fig. 4. Figure 4 shows that reflections from the superspheroidal radomes tend to shift the operating frequency of the antenna and to narrow the antenna's passband. The spherically blunted cone has the least impact on S_{11} in the passband and gives the most similar behavior to the antenna performance without a radome.

Figures 5 (a, b) compares the antenna radiation patterns for the H-plane and E-plane for each radome. Figure 5 (a) shows that the superspheroid with p=1.161 causes the highest deterioration in the main lobe of the H-plane radiation pattern (ϕ=270 deg). The ogive radome (p=1.449) has reduced the directivity of the main beam of antenna (ϕ=270 deg). The spherically blunted radome has the radiation pattern most similar to the antenna with no radome. All radomes cause the slight increase in the side lobe (ϕ=90 deg). Figure 5 (b) shows that in the E-plane, the superspheroid with p=1.161 has significantly increased the directivity of antenna whilst the ogive radome (p=1.449) has decreased the directivity in the E-plane. Again, the spherically blunted radome has the E-plane pattern most similar to the antenna with no radome.

Our analysis of the effect that different superspheroidal radome profiles have on the radiation pattern of the antenna are very different from those in [2] that reported only very minor differences in sidelobes of the antenna radiation. This is, we believe, due to the "decoupled" approach employed in [2].

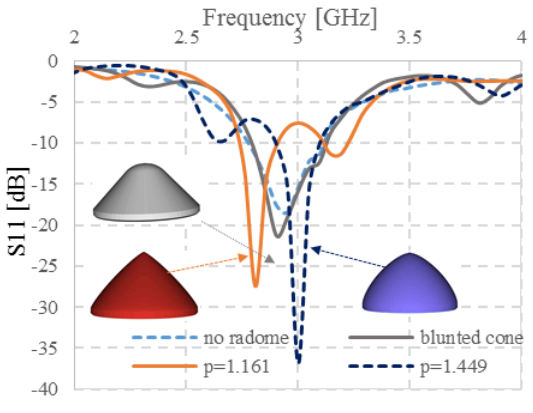

Fig. 4. Comparison of antenna S_{11} parameter in the presence of different radome profiles.

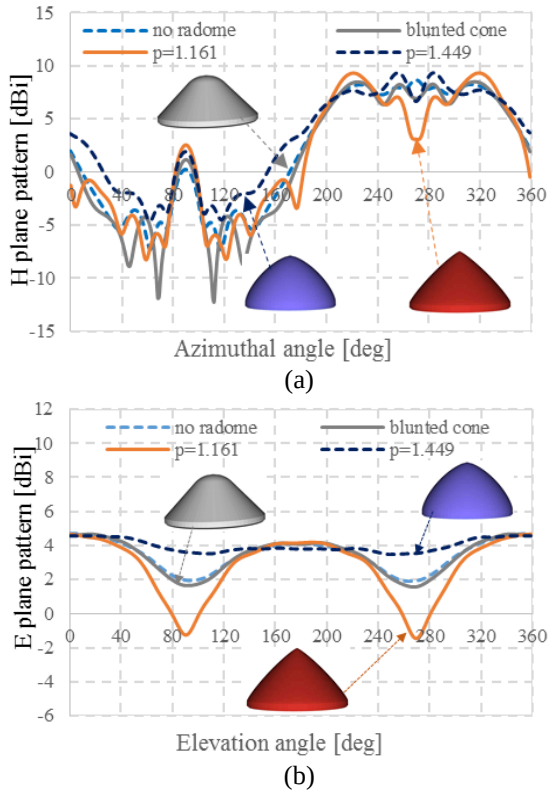

Fig. 5. Comparison of the antenna radiation pattern in the presence of different radomes for: (a) H-plane and (b) E-plane.

IV. CONCLUSION

The paper analyses broadband interactions between antennas installed in airborne radomes in a fully coupled manner by directly sampling both the antenna and the radome geometry using a single numerical method. In order to isolate the effect of the radome, the antenna's performance is first modelled in the presence of just the radome base. Two different superspheroidal radomes and the spherically blunted cone are then introduced and their impact on the antenna's performance assessed. The paper shows that a spherically blunted cone has the least influence on antenna's performance and that superspheroids can significantly change the antennas performance and need to be designed with care.

ACKNOWLEDGMENT

The authors wish to thank Dr. S. Earl and Prof. C. Jones of BAE SYSTEMS for many valuable discussions.

REFERENCES

[1] R. U. Nair and R. M. Jha, "Electromagnetic design and performance analysis of airborne radomes: Trends and perspectives," *IEEE Antennas and Prop. Magazine*, vol. 56, pp. 276-298, 2014.

[2] W.-J. Zhao, L.-W. Li, and Y.-B. Gan, "Efficient analysis of antenna radiation in the presence of airborne dielectric radomes of arbitrary shape," *IEEE Trans. Antennas and Prop*., vol. 53, pp. 442-448, 2005.

[3] P. Sewell, T. M. Benson, C. Christopoulos, D. W. P. Thomas, A. Vukovic, and J. G. Wykes, "Transmission line modeling (TLM) based upon unstructured tetrahedral meshes," *IEEE Trans. Microwave Theory and Tech*., vol. 53, pp. 1919-1928, 2005.

[4] P. Sewell, T. M. Benson, C. Christopoulos, D. W. P. Thomas, A. Vukovic, and J. G. Wykes, "Implicit element clustering for tetrahedral transmission-line modeling (TLM)," *IEEE Trans. Microw. Theory Tech.*, vol. 57, no. 6, pp. 2005-2014, June 2009.

[5] P. Sewell, J. G. Wykes, T. M. Benson, C. Christopoulos, D. W. P. Thomas, and A. Vukovic, "Multi-grid interface in computational electro-magnetics," *Electron. Lett*., vol. 40, pp. 162-163, 2004.

[6] A. E. Yilmaz, Z. Lou, E. Michielssen, and J. M. Jin, "A single boundary implicit and FFT-accelerated time-domain finite element-boundary integral solver," *IEEE Trans. Antennas and Propagat*., vol. 55, pp. 1382-1397, 2007.

[7] J. Shewchuk, Lecture notes on Delaunay Mesh Generation. https://people.eecs.berkeley.edu/~jrs/meshpapers/delnotes.pdf